# Exploring chemical reactions in a quantum degenerate gas of polar molecules via complex formation

Peiru He, <sup>1,2</sup> Thomas Bilitewski, <sup>1,2</sup> Chris H. Greene, <sup>3,4</sup> and Ana Maria Rey<sup>1,2</sup>

<sup>1</sup>JILA, National Institute of Standards and Technology and Department of Physics, University of Colorado, Boulder, Colorado 80309, USA <sup>2</sup>Center for Theory of Quantum Matter, University of Colorado, Boulder, Colorado 80309, USA <sup>3</sup>Department of Physics and Astronomy, Purdue University, West Lafayette, Indiana 47907, USA <sup>4</sup>Purdue Quantum Science and Engineering Institute, Purdue University, West Lafayette, Indiana 47907, USA

(Received 14 August 2020; revised 21 October 2020; accepted 9 November 2020; published 18 December 2020)

A recent experiment [L. De Marco, G. Valtolina, K. Matsuda, W. G. Tobias, J. P. Covey, and J. Ye, A degenerate Fermi gas of polar molecules, Science 363, 853 (2019)] reported for the first time the preparation of a Fermi degenerate gas of polar molecules and observed a suppression of their chemical reaction rate compared to the one expected from a treatment assuming classical Maxwell-Boltzmann statistics. While it was hypothesized that the suppression in the ultracold regime had its roots in the Fermi statistics of the molecules, this argument is inconsistent with the fact that the Fermi pressure should set a lower bound for the chemical reaction rate. Here we develop a simple model of chemical reactions that occur via the formation and decay of molecular complexes. We indeed find that pure two-body molecule losses are unable to explain the observed suppression. Instead we extend our description beyond two-body physics by including multibody complex-molecule interactions. Although our model is able to quantitatively reproduce recent experimental observations, it requires parameters physically unlikely for direct microscopic interactions. The underlying processes, however, might emerge effectively from many-body or medium effects. A detailed understanding of the direct microscopic mechanisms responsible for these higher-order interaction processes is therefore still pending.

#### DOI: 10.1103/PhysRevA.102.063322

# I. INTRODUCTION

Polar molecular gases, offering tunable long-range interactions and a large set of internal degrees of freedom, are an ideal platform to explore a wide range of many-body phenomena that are difficult to access in atomic systems. The prerequisite for many of these explorations is the preparation of quantum degenerate samples, which has been one of the most challenging goals in molecular physics over past decades [1–5]. Major challenges arise due to the complex molecular internal structure and the rapid loss caused by chemical reactions which prevent the application of standard cooling techniques for atoms [2,6].

The use of spin-polarized fermionic molecules facilitated experimental efforts to reduce the undesirable chemical reactions as in these systems the collisions are dominated by p-wave scattering. In this case, according to the Bethe-Wigner threshold law [7-9], chemical reactions are partially suppressed by the centrifugal barrier resulting in a loss rate that scales linearly with temperature T. A quantitative analysis using a multichannel quantum defect theory (MQDT) [10,11] captured this behavior with a universal decay constant which well explained the experimentally observed decay rate in a gas of KRb molecules prepared in the classical regime where the Fermi statistics is well approximated by Boltzmann statistics  $(T > 0.5T_F)$ , with  $T_F$  the Fermi temperature) [1,6]. However, the Bethe-Wigner threshold law has been shown to fail in a recent experiment [1] which prepared for the first time a quantum degenerate gas of KRb molecules in a three-dimensional

(3D) dipole trap reaching temperatures below  $0.3T_F$ . Deep in the quantum degenerate limit ( $T < 0.5T_F$ ), a significant suppression of the loss rate compared to the one predicted by the MQDT theory was observed and conjectured to be a consequence of the underlying Fermi statistics. Yet, this explanation is inconsistent with the naive expectation that, as the temperature vanishes, the Fermi pressure sets a lower bound for the p-wave reaction rate, which would instead lead to a rate higher than the one predicted by arguments based on classical Maxwell-Boltzmann statistics. The observed suppression therefore requires an explanation more profound than just Fermi statistics.

Recent experiments [12,13] moreover revealed that even in reactive molecules such as KRb, chemical reactions occur via the formation of a transient complex whose properties may affect the collision outcome. These observations therefore have opened the possibility of richer chemical reaction processes [14].

Here we provide a possible explanation of the observed chemical reaction suppression at ultracold temperatures by developing a theoretical many-body framework that accounts for the formation of molecular complexes. The large decay rate of the complex [12,13] allows us to adiabatically eliminate the complex, and obtain an effective two-body decay of the molecules which recovers the standard description of KRb chemical reactions. We analytically solve the rate equations, accounting for both heating effects and quantum Fermi statistics. We obtain a decay rate that is in agreement with the Bethe-Wigner threshold laws above quantum degeneracy,

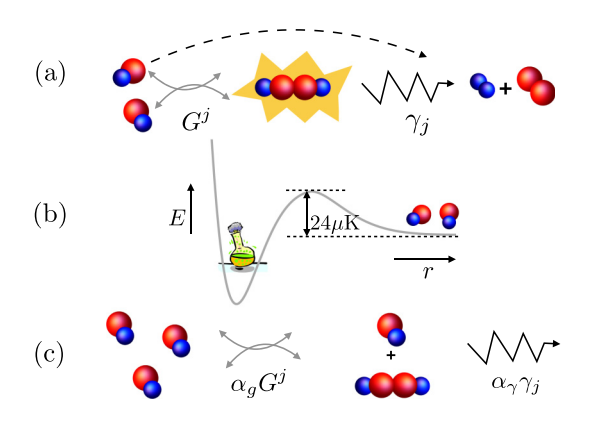


FIG. 1. Schematics of the reactive collision processes. (a) Two KRb molecules coherently collide in the p-wave channel with rate  $G^j$  to form an intermediate complex  $K_2Rb_2$ , which subsequently decays to the reaction products  $K_2$  and  $Rb_2$  at a rate  $\gamma_j$ . If the complex decay rate  $\gamma_j$  is the fastest process, as for KRb molecules, the complex can be adiabatically eliminated, giving rise to an effective two-body decay. (b) This recovers the standard picture of direct chemical reactions via p-wave inelastic collisions, where chemical reactions occur with unit probability at short range inside the centrifugal barrier. (c) Additional (in)elastic complex-molecule collisions with rate  $\alpha_g G^j(\alpha_\gamma \gamma_j)$  effectively generate three-body molecule processes which can suppress the two-body molecule decay rate.

and also valid in the ultracold quantum regime. However, this model fails to capture the experimental observations in the quantum degenerate regime. We therefore turn to an effective description, modeling beyond two-body physics by including effective elastic and inelastic complex-molecule interactions possibly emerging from many-body and effective medium effects at finite densities and in the presence of trapping light, which can generate a loss suppression mechanism like that observed in the experiment.

# II. THE MODEL

We begin by deriving a framework including an intermediate complex, whose existence has recently been experimentally demonstrated [12,13], formed via the collision of two molecules as illustrated in Fig. 1(a), which recovers standard chemical reaction rate equations.

We consider N fermionic molecules, with mass m confined by an external potential V(r), which for simplicity we first set to be a simple square well that defines a confinement volume V. In this system momentum  $\hbar \mathbf{k}$  is a good quantum number. For molecules prepared in a single internal quantum state, p-wave scattering dominates the collisions at ultracold temperatures due to Fermi statistics, which is, thus, the only partial wave we include. Assuming there are multiple channels to form a complex (each denoted by j) the collision processes can be modeled by a simplified master equation

$$\frac{d\hat{\rho}}{dt} = \frac{i}{\hbar} [\hat{H}, \, \hat{\rho}] + \mathcal{L}(\hat{\rho}), \quad \hat{H} = \hat{H}_{\text{single}} + \hat{H}_{\text{int}}, \quad (1)$$

$$\hat{H}_{\text{single}} = \sum_{j,k} E_{j,k}^b \hat{b}_{j,k}^{\dagger} \hat{b}_{j,k} + \sum_{k} E_k^c \hat{c}_k^{\dagger} \hat{c}_k, \qquad (2)$$

$$\hat{H}_{\text{int}} = \sum_{j,k,k'} \frac{\hbar g_j}{\sqrt{V}} |k - k'| (\hat{b}_{j,k+k'}^{\dagger} \hat{c}_k \hat{c}_{k'} + \text{H.c.}), \quad (3)$$

$$\mathcal{L}(\hat{\rho}) = \sum_{j,k} \gamma_j \mathcal{L}[\hat{b}_{j,k}] \,\hat{\rho},\tag{4}$$

where  $\hat{c}_k^\dagger$  ( $\hat{c}_k$ ) is a fermionic creation (annihilation) operator of a molecule with momentum  $\hbar k$ ,  $\hat{b}_{j,k}^\dagger$  ( $\hat{b}_{j,k}$ ) is a bosonic creation (annihilation) operator of a complex formed via channel j,  $E_k^c = \hbar^2 k^2/(2m)$  and  $E_{j,k}^b = \hbar^2 k^2/(4m) + E_j$  are the single-particle energies of the molecules and complexes, respectively, with  $E_j$  the binding energy of a complex. Without loss of generality, we do not explicitly include the internal states and energies of the particles. Adding them does not change any of the conclusions under the large complex loss rate assumption used in this work (see Appendix C). The parameter  $g_j$  sets the complex-molecule collision strength and  $\gamma_j$  is the complex decay rate. The Lindblad term  $\mathcal{L}[\hat{O}]\hat{\rho} = \hat{O}^\dagger\hat{\rho}\,\hat{O} - \frac{1}{2}(\hat{\rho}\,\hat{O}^\dagger\hat{O} + \hat{O}^\dagger\hat{O}\hat{\rho})$  describes the action of an operator  $\hat{O}$  on the density matrix  $\hat{\rho}$  of the complex-molecule many-body system.

From the master equation one can obtain equations of motion of the relevant observables. Since for the problem of interest the initial state has zero coherence terms  $\langle \hat{c}_k^{\dagger} \hat{c}_{k'} \rangle = 0$  and  $\langle \hat{c}_k \hat{c}_{k'} \rangle = 0$  for  $k \neq k'$ , these terms can be neglected during the dynamics giving rise to the following equations:

$$\frac{d\langle \hat{n}_{k}\rangle}{dt} = \sum_{j,k'} 2G_{k,k'}^{j} \operatorname{Im}[\langle \hat{b}_{j,k+k'}^{\dagger} \hat{c}_{k} \hat{c}_{k'}\rangle], \tag{5}$$

$$\frac{d\langle \hat{b}_{j,k+k'}^{\dagger} \hat{c}_{k} \hat{c}_{k'} \rangle}{dt} = i \left( \frac{\hbar |\mathbf{k} - \mathbf{k}'|^{2}}{4m} - E_{j} / \hbar + i \gamma_{j} \right) \langle \hat{b}_{j,k+k'}^{\dagger} \hat{c}_{k} \hat{c}_{k'} \rangle 
+ i G_{k,k'}^{j} \left( \left\langle \hat{n}_{j,k+k'}^{b} \right\rangle - 2 \langle \hat{n}_{k} \hat{n}_{k'} \rangle \right), \tag{6}$$

$$\frac{d\langle \hat{n}_{j,k}^b \rangle}{dt} = -2\gamma_j \langle \hat{n}_{j,k}^b \rangle - G_{k,k-k'}^j \operatorname{Im}[\langle \hat{b}_{j,k}^\dagger \hat{c}_{k'} \hat{c}_{k-k'} \rangle] \quad (7)$$

with  $\hat{n}_k = \hat{c}_k^{\dagger} \hat{c}_k$ ,  $\hat{n}_{j,k}^b = \hat{b}_{j,k}^{\dagger} \hat{b}_{j,k}$ , and  $G_{k,k'}^j = \frac{2g_j}{\sqrt{\nu}} |k-k'|$ . The mean complex decay rate  $\overline{\nu}$  has been measured to be  $2\pi \times 4$  MHz in free space and even larger in the presence of trapping light [13]. Because this rate is much larger than any other energy scales of the molecular gas [1], the complex associated observables reach their steady state much faster than any other dynamical processes occurring in the molecules. As a consequence, we can adiabatically eliminate the complex, i.e., set the left-hand side of Eqs. (6) and (7) to zero, solve for the steady-state values of  $\langle \hat{n}_{j,k}^b \rangle$  and  $\langle \hat{b}_{j,k+k'}^{\dagger} \hat{c}_k \hat{c}_{k'} \rangle$ , and replace them back into the equations of motion of the molecules. Note that since the steady-state value of  $\langle \hat{n}_{j,k}^b \rangle$  is much smaller than  $\langle \hat{n}_{j,k} \rangle$  we can neglect it. The complex-molecule coherence term then obeys (see details in Appendix A):

$$\langle \hat{b}_{j,k+k'}^{\dagger} \hat{c}_{k} \hat{c}_{k'} \rangle \approx -i \frac{2G_{k,k'}^{j}}{(\gamma_{j} - iE_{j}/\hbar)} \langle \hat{n}_{k} \hat{n}_{k'} \rangle$$

$$\approx -i \frac{2G_{k,k'}^{j}}{(\gamma_{j} - iE_{j}/\hbar)} \langle \hat{n}_{k} \rangle \langle \hat{n}_{k'} \rangle. \tag{8}$$

The factorization used above,  $\langle \hat{n}_k \hat{n}_{k'} \rangle = \langle \hat{n}_k \rangle \langle \hat{n}_{k'} \rangle$ , is based on a mean-field approximation which neglects quantum

fluctuations. Corrections to this approximation could in principle modify the loss rate equations. However, for the initial conditions and parameters used in the experiment, we find corrections from quantum fluctuations are completely negligible (see Appendix B) and the mean-field assumption to be a good approximation. After replacing Eq. (8) with Eq. (5) one recovers the standard equations that describe direct chemical reactions, if we identify the p-wave collision parameters in terms of the real and imaginary parts of the scattering volume  $b_{\mathrm{im,re}}^3$  as follows:  $g_{\text{im}} \equiv 3\pi \hbar b_{\text{im}}^3/m = \sum_j 4g_j^2 \gamma_j/[\gamma_j^2 + (E_j/\hbar)^2]$  and  $g_{\rm re} \equiv 3\pi \hbar b_{\rm re}^3/m = \sum_j 4g_j^2 (E_j/\hbar)/[\gamma_j^2 + (E_j/\hbar)^2]$  (see details in Appendix A). The real part describes elastic collisions that thermalize the system, and the imaginary part gives rise to the reactive collision rate [15] as illustrated in Fig. 1(b). We observe that in the limit of a large decay rate  $\gamma_i \gg g_i$ , we are in the quantum Zeno regime [16-18] where the decay of the molecules is limited by the formation of the complex, and in fact, is suppressed with increasing  $\gamma_j$ . We also note that in this limit the single-particle energies do not play a role.

We find that the dynamics of the particle decay is mainly determined by the inelastic part since the elastic collisions conserve the total particle number and only slightly affect the decay rate by redistributing the mode population (see details in Appendix D). Thus, in the following discussion, for simplicity we set  $g_{\rm re} = 0$ . In this case the corresponding rate equations simplify to

$$\frac{d\langle \hat{n}_{k}\rangle}{dt} \approx -\sum_{k'} \Gamma_{kk'} \langle \hat{n}_{k}\rangle \langle \hat{n}_{k'}\rangle, \tag{9}$$

with  $\Gamma_{k,k'} = 4g_{\rm im}|\mathbf{k} - \mathbf{k'}|^2/V$ . The complex population adiabatically follows the molecule population as  $\langle \hat{n}_{j,k}^b \rangle \approx \sum_{k'} \Gamma_{kk'}/(2\gamma_j) \langle \hat{n}_k \rangle \langle \hat{n}_{k'} \rangle$ .

We can easily generalize Eq. (9) to any type of trapping potential V(r) by considering the corresponding single-particle eigenmodes. Explicitly,

$$\frac{d\langle \hat{n}_{n}\rangle}{dt} \approx -\sum_{n'} \Gamma_{nn'} \langle \hat{n}_{n}\rangle \langle \hat{n}_{n'}\rangle, \tag{10}$$

$$\frac{dN}{dt} = -\sum_{n} \frac{d\langle \hat{n}_{n} \rangle}{dt} \equiv -\overline{\Gamma} N^{2}, \tag{11}$$

where  $\hat{n}_n = \hat{c}_n^{\dagger} \hat{c}_n$  denotes the molecule population operator in mode n,  $\Gamma_{nn'}$  is given by an integral over eigenmodes n and n' (see details in Appendix A), and we defined the time-dependent averaged particle decay rates as  $\overline{\Gamma} = \sum \Gamma_{nn'} \langle \hat{n}_n \rangle \langle \hat{n}_{n'} \rangle / N^2$ .

#### III. COMPARISON WITH EXPERIMENT

We now apply this developed framework to the experimental conditions, assuming a 3D harmonic trapping potential of the form  $V(\mathbf{r}) = \sum_{i=x,y,z} m\omega_i^2 r_i^2/2$  with  $\omega_i$  the trapping frequency in the ith direction. In addition to the total particle number N(t), we study the density  $n \equiv N/V$ , the volume V, defined as  $V = 8\pi^{3/2}(\sigma_x\sigma_y\sigma_z)$  with  $\sigma_i$  the standard deviation of the density profile in the ith direction, the total energy E, and the energy density  $\epsilon \equiv E/N$ .

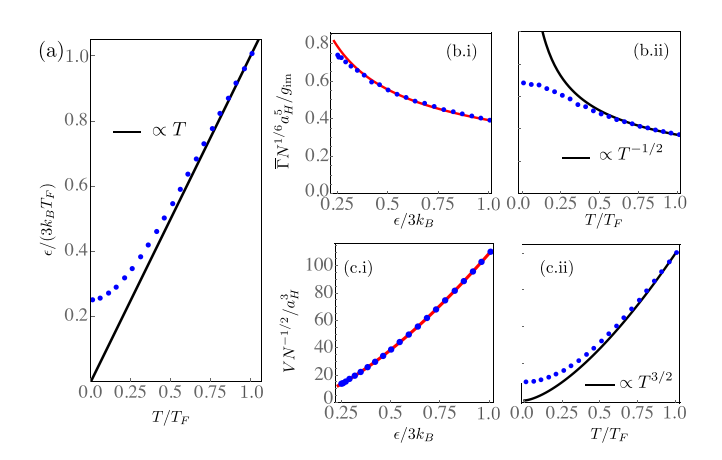


FIG. 2. Thermodynamic scaling relations in a 3D harmonic trap: (a) average energy density,  $\epsilon$ , (b)  $\overline{\Gamma}$ , and (c) average volume, V. Numerical results are shown as blue dots, and analytical scalings as a function of energy density [red lines (b.i) and (c.i)] and temperature [black lines (b.ii) and (c.ii)]. Only the scaling in terms of  $\epsilon$  remains valid in the quantum degenerate regime.

Note that the effective loss rate Eq. (10) for the molecules takes exactly the same form as the original rate equation derived assuming direct molecule-molecule scattering. Indeed, generically both channels are present as recently shown in Ref. [14]. Since so far there is no way to identify the individual contributions from these processes, for simplicity, we assume the loss comes purely from the complex-molecule scattering. We therefore equate the effective molecule loss rate resulting from this process to the one measured experimentally [1], which was assumed to be set by a p-wave scattering volume  $b_{\rm im}^3 = (118a_0)^3$  with  $a_0$  the atomic Bohr radius.

To develop an analytical understanding, we explore the scaling relations of the averaged decay rates and the volume. For an equilibrium system at temperature T, the population  $\langle \hat{n}_n \rangle$  obeys the Fermi-Dirac distribution, from which the energy density  $\epsilon$ ,  $\overline{\Gamma}$ , and V can be obtained as a function of T. As shown in Fig. 2(a), in the classical limit  $T \gtrsim 0.5T_F$ , the energy density  $\epsilon$  in each direction is  $k_BT$  in the harmonic trap in accordance with the equipartition theorem, giving rise to  $\epsilon = 3k_BT$ ; in the quantum degenerate limit  $T \lesssim 0.5T_F$ ,  $\epsilon$ is higher than the one predicted by a classical scaling since the Fermi energy remains finite at zero temperature due to quantum statistics. As demonstrated in Fig. 2(b), the scaling relations  $\overline{\Gamma} \propto \epsilon^{-1/2}$  and  $V \propto \epsilon^{3/2}$ , written as a function of  $\epsilon$ , are universal over the whole temperature range, whereas only in the classical regime the replacement  $\epsilon \to T$  is valid as shown in Figs. 2(b.ii) and 2(c.ii).

During the nonequilibrium decay dynamics these simple relations derived in equilibrium are not necessarily applicable. Notwithstanding, they are found to keep holding during the full dynamics as benchmarked by numerical simulations (see details in Appendix F). We attribute this partly to the fact that in a harmonic trap the initial Fermi distribution remains approximately unchanged during the dynamics by the balancing between the local density and the *p*-wave decay rate: the lowenergy modes with a low *p*-wave decay rate concentrate at the trap center where the density is higher, while the high-energy

modes with faster decay rates concentrate at the edges where the density is lower, making the effective decay rate nearly uniform through the cloud.

In the experiment there is additional heating as particles are lost (see details in Appendix E) similar to that observed in prior experiments [19,20]. Here we phenomenologically describe these heating processes by a background single-particle heating rate  $3k_Bh_{\rm bg}$  acting as

$$\frac{dN}{dt} = -\overline{\Gamma}N^2, \quad \frac{d\epsilon}{dt} = 3k_B h_{\rm bg},\tag{12}$$

where  $V = V_0(\epsilon/\epsilon_0)^{3/2}$  and  $\overline{\Gamma} = \overline{\Gamma}_0(\epsilon/\epsilon_0)^{-1/2}$ , and the subscript 0 denotes the values at t = 0. The dynamics of the density n(t) can be analytically obtained as

$$n(t) \approx \frac{n_0 (1 + 3k_B ht/\epsilon_0)^{-3/2}}{1 + 2\overline{\Gamma}_0 V_0 n_0 \sqrt{\epsilon_0} (\sqrt{\epsilon_0 + 3k_B ht} - \sqrt{\epsilon_0})/(3k_B h)}.$$
(13)

From this expression the density decay rate, which was the fitting parameter used to characterize the decay rate in Ref. [1], is predicted to be at short times  $\beta_0 \equiv \overline{\Gamma}_0 V_0 \propto \epsilon_0$ , and thus proportional to the energy density. In the classical limit, this recovers the results of the Bethe-Wigner threshold law since  $\epsilon = 3k_BT$ . In the quantum degenerate limit, the decay rate saturates to the Fermi energy  $k_BT_F$  instead of decreasing to zero.

To directly compare with the experimentally extracted rates, we numerically extract the decay rate  $\beta_0$  as the best fit of n(t) to Eq. (13) for the corresponding initial conditions (see Appendix I for detailed fitting procedures). As shown in Fig. 3, the theory results are flat throughout both the classical temperature and the quantum degenerate regime, while the experimental data shows a strong suppression in the latter. We note that both represent an enhancement compared to the prediction for a classical gas for which the decay rate would vanish in the zero-temperature limit. Thus, we find that for a spin-polarized gas there is no suppression of losses due to Fermi statistics or antibunching in the quantum degenerate regime and that a different mechanism is required to explain the experimental observed suppression.

#### IV. BEYOND TWO-BODY MOLECULE LOSS

Having established that pure two-body molecule decay is insufficient to explain the experimentally observed suppression, we consider more complicated interaction processes in our model. The net loss rate of molecules in our framework can be modified by additional complex-molecule collisions as we show next. We explore both elastic and inelastic collisions between molecules and complexes, as illustrated in Fig. 1(c).

To connect to Eq. (4), for simplicity we start again by considering a homogeneous gas and model these processes by adding the following terms in the master equation:

$$\hat{H}'_{\text{int}} = \sum_{j,k,k',k''} \frac{\hbar \alpha_g}{2V} G^j_{k,k'} (\hat{b}^{\dagger}_{j,k'+k''} \hat{c}^{\dagger}_{k} \hat{c}_{k} \hat{c}_{k'} \hat{c}_{k''} + \text{H.c.}),$$

$$\mathcal{L}'(\hat{\rho}) = \alpha_{\gamma} \sum_{j,k,k'} \gamma_{j} \mathcal{L}[\hat{b}_{j,k} \hat{c}_{k'}] \hat{\rho}/V,$$
(14)

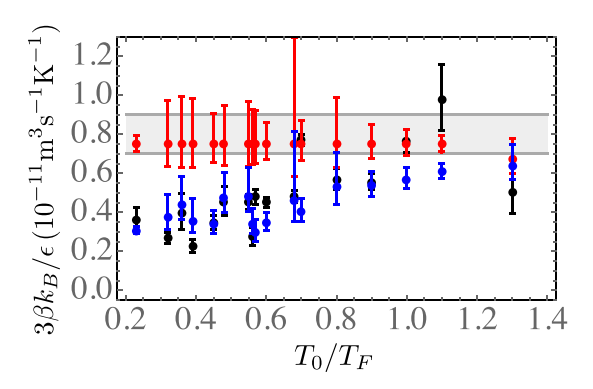


FIG. 3. Comparison of theory predictions considering pure pwave molecule-molecule collisions without (red dots) or with (blue dots) additional complex-molecule collisions assuming  $\alpha = 8 \times$ 10<sup>-20</sup> m<sup>3</sup>, and experimental measurements (black dots). Each dot corresponds to different experimental runs with slightly different conditions (see details in Appendix I). The theory (experiment)  $\beta_0/(\epsilon/3k_B)$  is obtained as the best fit of the theoretically derived (the experimentally measured) n(t) to Eq. (13). The error bars include uncertainties in the experimental measurements and the standard deviation from the fitting procedure (see details in Appendix I). In the classical temperature limit, both the theory and the experimental results are approximately constant, in agreement with the universal prediction [11] indicated by the gray band accounting for 8% errors in the scattering value  $b_{\text{im}}^3$ . In the quantum degenerate limit, the model including the complex-molecule collisions can quantitatively reproduce the observed suppression.

where the parameters  $\alpha_g G_{k,k'}^j/V$  and  $\alpha_\gamma \gamma_j/V$ , which have the unit of s<sup>-1</sup>, parametrizes the rates of three-body elastic collisions and the molecule-complex decay, respectively. After adiabatically eliminating the complex, these terms result in a modification of the two-body decay rate and an additional molecular three-body decay term (see details in Appendix G)

$$\frac{d\langle \hat{n}_{k}\rangle}{dt} \approx -\sum_{k'} \frac{(1+2\alpha_{g}n)}{(1+\alpha_{\gamma}n)} \Gamma_{k,k'} \langle \hat{n}_{k}\rangle \langle \hat{n}_{k'}\rangle 
-\sum_{i,k',k''} \frac{\alpha_{\gamma}}{2V} \Gamma_{k',k''} \langle \hat{n}_{k}\rangle \langle \hat{n}_{k'}\rangle \langle \hat{n}_{k''}\rangle,$$
(15)

where  $n = \sum_{k''} \langle \hat{n}_{k''} \rangle / V = N/V$  is the density of the molecular gas and we assumed  $E_j \ll \gamma_j$ . Consequently, the total number of molecules follows

$$\frac{dN}{dt} \approx -\sum_{\mathbf{k},\mathbf{k}'} \Gamma_{\mathbf{k},\mathbf{k}'}^{P} \langle \hat{n}_{\mathbf{k}} \rangle \langle \hat{n}_{\mathbf{k}'} \rangle, \tag{16}$$

where the modified decay rate becomes  $\Gamma^P_{k,k'} \equiv \Gamma_{k,k'}[1+(2\alpha_g-\alpha_\gamma/2)n]$ , with an effective inelastic scattering parameter  $g^P_{\rm im} \equiv g_{\rm im}(1-\alpha n)$  and  $\alpha=\alpha_\gamma/2-2\alpha_g$ . Thus, counterintuitively the additional loss due to complex-molecule collisions results in an effective suppression of the two-body loss due to the quantum Zeno effect which suppresses the population of the complex for larger loss rates.

For a gas trapped in a 3D harmonic potential this density-dependent scattering strength  $g_{\text{im}}^P$  generates an effective loss suppression in the quantum degenerate regime if  $\alpha > 0$  as the

gas becomes denser with decreasing temperature. In a system with a fixed particle number, where the change in density is directly correlated with the average volume, this suppression of the decay rate is tied to the temperature dependence of the average volume [see Fig. 2(c)], reflecting the underlying Fermi statistics.

In Fig. 3 we demonstrate that this effective model can reproduce the experimentally observed suppression when choosing  $\alpha = 8 \times 10^{-20}$  m<sup>3</sup> (see details in Appendix H). However, we note that this corresponds to an inelastic collision rate  $\alpha_{\gamma} \overline{\gamma} \sim 2 \times 10^{-12} \text{ m}^3/\text{s}$  between molecules and the complex which exceeds the unitary limit given by  $\sim 10^{-16}$  m<sup>3</sup>/s. Therefore these processes can only be regarded as phenomenological effective processes possibly emerging from indirect medium or many-body effects instead of direct microscopic collisions. In contrast, the elastic term  $\alpha_{g}g$  is in principle feasible, but requires a coherent three-body process, rather than the conventionally expected pure loss in a threebody collision [21,22]. A full explanation of the underlying many-body framework responsible for the emergence of this term, either from quasiparticle dressing and in medium interactions, or direct multibody or light assisted collisions is still pending.

#### V. CONCLUSIONS AND OUTLOOK

We have developed a theoretical framework that accounts for the formation of an intermediate molecular complex to study the reactive dynamics of a quantum degenerate gas of polar molecules. The first part of this work considering pure *p*-wave collision of the molecules establishes a decay rate proportional to the energy density of the gas, extending the Wigner threshold law to the quantum degenerate regime where the fermionic statistics of the particles become

relevant, and predicts a flat behavior at low temperature enhanced compared to the linearly in T vanishing prediction obtained for Maxwell-Boltzmann statistics. Thus, we find no suppression of losses due to Fermi statistics or antibunching in the quantum degenerate regime at current experimental conditions when quantum correlations are negligible. As two-body molecule decay processes mediated by the formation of complexes alone do not reproduce the experimentally observed behavior in the quantum degenerate regime, we considered beyond two-body molecule collisions. By including elastic or inelastic higher order complex-molecule interactions we are able to reproduce the experimental observations. Nevertheless, it seems unlikely that the actual origin of these terms is direct complex-molecule collisions. Instead they may emerge from many-body effects in the presence of trapping light. We hope that our conclusions can stimulate further theory work for an understanding of the microscopic origin of these effects and experimental work that can directly validate or refute our predictions.

#### **ACKNOWLEDGMENTS**

We acknowledge helpful discussions with Jun Ye and his JILA KRb group, Joseph Thywissen, Paul Julienne, John Bohn, and Qi Zhou during the preparation of this paper. This work is supported by the ARO single investigator Award No. W911NF-19-1-0210, the DARPA DRINQs program, and the JILA-PFC PHY-1734006 grants, by NIST, and by NSF Grant No. PHY-1912350.

# APPENDIX A: DERIVATIONS OF THE RATE EQUATIONS

Here we first derive the equations of motion described by Eqs. (1)–(4) in the main text. We define  $\hat{A}_{k,k'} = \hat{a}_k \, \hat{a}_{k'}$  and  $\hat{C}_{k,k'} = \hat{a}_k^{\dagger} \, \hat{a}_{k'}$ .

$$\frac{d \langle \hat{b}_{k,j}^{\dagger} \hat{b}_{k',j'} \rangle}{dt} = i \left( -E_{j}/\hbar + E_{j'}/\hbar + \frac{\hbar |\mathbf{k}'|^{2} - \hbar |\mathbf{k}|^{2}}{4m} \right) \langle \hat{b}_{k,j}^{\dagger} \hat{b}_{k',j'} \rangle - (\gamma_{j} + \gamma_{j'}) \langle \hat{b}_{k,j}^{\dagger} \hat{b}_{k',j'} \rangle$$

$$+ \frac{i}{\sqrt{V}} \sum_{\mathbf{k''}} (g_{j'} | 2\mathbf{k''} - \mathbf{k'} | \langle \hat{b}_{k,j}^{\dagger} \hat{A}_{k'',k'-k''} \rangle - g_{j} | 2\mathbf{k''} - \mathbf{k} | \langle \hat{A}_{k'',k-k''}^{\dagger} \hat{b}_{k',j'} \rangle), \qquad (A1)$$

$$\frac{d \langle \hat{A}_{k,k'} \rangle}{dt} = i \frac{\hbar |\mathbf{k}|^{2} + \hbar |\mathbf{k'}|^{2}}{2m} \langle \hat{A}_{k,k'} \rangle + i \frac{2}{\sqrt{V}} \sum_{j} g_{j} |\mathbf{k} - \mathbf{k'} | \langle \hat{b}_{k+k',j} \rangle$$

$$+ i \frac{2}{\sqrt{V}} \sum_{\mathbf{k''},j} g_{j} (|\mathbf{k''} - \mathbf{k}| \langle \hat{C}_{k'',k'} \hat{b}_{k''+k,j} \rangle) + |\mathbf{k'} - \mathbf{k''} | \langle \hat{C}_{k'',k} \hat{b}_{k''+k',j} \rangle), \qquad (A2)$$

$$\frac{d \langle \hat{b}_{\mathbf{k''},j}^{\dagger} \hat{A}_{k,k'} \rangle}{dt} = i \left( \frac{2\hbar |\mathbf{k}|^{2} + 2\hbar |\mathbf{k'}|^{2} - \hbar |\mathbf{k''}|^{2}}{4m} - E_{j} / \hbar \right) \langle \hat{b}_{k'',j}^{\dagger} \hat{A}_{k,k'} \rangle - \gamma_{j} \langle \hat{b}_{k'',j}^{\dagger} \hat{A}_{k,k'} \rangle$$

$$+ i \frac{2}{\sqrt{V}} \sum_{j} g_{j'} |\mathbf{k} - \mathbf{k'} | \langle \hat{b}_{k'',j}^{\dagger} \hat{b}_{k+k',j'} \rangle - i \frac{2}{\sqrt{V}} \sum_{k'''} g_{j} |2\mathbf{k'''} - \mathbf{k''} | \langle \hat{A}_{k''',k''-k'''}^{\dagger} \hat{A}_{k,k'} \rangle$$

$$+ i \frac{2}{\sqrt{V}} \sum_{j} g_{j'} (|\mathbf{k'''} - \mathbf{k}| \langle \hat{b}_{k'',j}^{\dagger} \hat{C}_{k''',k} \hat{b}_{k'''+k,j'} \rangle + |\mathbf{k'} - \mathbf{k'''} | \langle \hat{b}_{k'',j}^{\dagger} \hat{C}_{k''',k} \hat{b}_{k'''+k',j'} \rangle), \qquad (A3)$$

$$\frac{d \langle \hat{C}_{k,k'} \rangle}{dt} = i \frac{\hbar |\mathbf{k'}|^{2} - \hbar |\mathbf{k}|^{2}}{2m} \langle \hat{C}_{k,k'} \rangle + i \frac{2}{\sqrt{V}} \sum_{j,k''} g_{j} (|\mathbf{k} - \mathbf{k''} | \langle \hat{b}_{k'''+k,j}^{\dagger} \hat{A}_{k'',k'} \rangle + |\mathbf{k''} - \mathbf{k'} | \langle \hat{A}_{k'',k}^{\dagger} \hat{b}_{k''+k',j} \rangle), \qquad (A4)$$

$$\frac{d\langle \hat{C}_{k,k'} \hat{b}_{k'',j} \rangle}{dt} = i \left( \frac{2\hbar |\mathbf{k}'|^2 - 2\hbar |\mathbf{k}|^2 + \hbar |\mathbf{k}''|^2}{4m} + E_j/\hbar + i\gamma_j \right) \langle \hat{b}_{j,k''} \hat{C}_{k,k'} \rangle + i \frac{2}{\sqrt{V}} \sum_{k'''} g_j |2k''' - k''| \langle \hat{C}_{k,k'} \hat{A}_{k''',k''-k'''} \rangle 
+ i \frac{2}{\sqrt{V}} \sum_{j',k'''} g_{j'} \left( |\mathbf{k} - \mathbf{k}'''| \langle \hat{b}_{k'''+k,j'}^{\dagger} \hat{A}_{k''',k'} \hat{b}_{k'',j} \rangle + |\mathbf{k}''' - \mathbf{k}'| \langle \hat{A}_{k''',k}^{\dagger} \hat{b}_{k'''+k',j'} \hat{b}_{k'',j} \rangle \right).$$
(A5)

Assuming the observables can be factorized as

$$\langle \hat{A}_{k_{1},k_{2}} \hat{A}_{k_{3},k_{4}}^{\dagger} \rangle = \langle \hat{A}_{k_{1},k_{2}} \rangle \langle \hat{A}_{k_{3},k_{4}}^{\dagger} \rangle - (\langle \hat{C}_{k_{4},k_{1}}^{\dagger} \rangle - \delta_{k_{1},k_{4}}) (\langle \hat{C}_{k_{3},k_{2}} \rangle - \delta_{k_{2},k_{3}}) 
+ (\langle \hat{C}_{k_{3},k_{1}}^{\dagger} \rangle - \delta_{k_{1},k_{3}}) (\langle \hat{C}_{k_{4},k_{2}} \rangle - \delta_{k_{2},k_{4}}),$$
(A6)

$$\langle \hat{C}_{k_1,k_2} \hat{A}_{k_3,k_4}^{\dagger} \rangle = \langle \hat{C}_{k_1,k_2} \rangle \langle \hat{A}_{k_3,k_4}^{\dagger} \rangle - (\langle \hat{C}_{k_4,k_1}^{\dagger} \rangle - \delta_{k_1,k_4}) (\langle \hat{C}_{k_3,k_2} \rangle - \delta_{k_2,k_3})$$

$$+ (\langle \hat{C}_{k_3,k_4}^{\dagger} \rangle - \delta_{k_1,k_3}) (\langle \hat{C}_{k_4,k_5} \rangle - \delta_{k_2,k_4}),$$
(A7)

then the equations of motion above become a closed set of equations and the dynamics of the observables can be evaluated. Our numerical simulations confirm the coherence terms  $\langle \hat{A}_{k_1,k_2} \rangle$ ,  $\langle \hat{C}_{k_1,k_2} \rangle$   $(k_1 \neq k_2)$  and  $\langle \hat{b}_{k_3,j}^{\dagger} \hat{A}_{k_1,k_2} \rangle$   $(k_3 \neq k_1 + k_2)$ , which are initially zero, remain zero, and therefore can be neglected. Then the relevant observables are  $\langle \hat{C}_{k_1,k_1} \rangle$ ,  $\langle \hat{b}_{k_j}^{\dagger} \hat{b}_{k_{j'}} \rangle$ , and  $\langle \hat{b}_{k_1,k_2}^{\dagger} \rangle$ .

and  $\langle \hat{b}^{\dagger}_{k_1+k_2,j} \hat{A}_{k_1,k_2} \rangle$ . In Ref. [13], the lifetime of the KRb complex was measured to be  $\gtrsim 250$  ns, indicating the mean decay rate  $\overline{\gamma_j} \gtrsim 2\pi \times 4$  MHz. Since the experimentally relevant energy scales are set by the Fermi energy (approximately kHz), which is much smaller than the complex decay rate, we can adiabatically eliminate the complex, and set to zero both the left-hand side of Eq. (A3) and the term  $\langle \hat{b}^{\dagger}_{j,k+k'} \hat{b}_{j,k+k'} \rangle$ . Then the correlation terms can be approximated as

$$\langle \hat{b}_{j,k+k'}^{\dagger} \hat{A}_{k,k'} \rangle \approx -i \frac{4g_j}{\sqrt{V}} |\mathbf{k} - \mathbf{k}'| \langle \hat{n}_k \hat{n}_{k'} \rangle / (\gamma_j - i E_j / \hbar)$$

$$\approx -i \frac{4g_j}{\sqrt{V}} |\mathbf{k} - \mathbf{k}'| \langle \hat{n}_k \rangle \langle \hat{n}_{k'} \rangle / (\gamma_j - i E_j / \hbar), \quad (A8)$$

where  $\hat{n}_k = \hat{c}_k^{\dagger} \hat{c}_k$ . We will discuss in detail about validity of the mean-field approximation (the second approximation here) in Appendix B. Here we have also ignored single-particle kinetic energy terms since they are in the order of  $\sim$ kHz  $\ll \gamma_j \sim$  MHz. By substituting the correlations into Eq. (A4), the dynamics for the molecular population becomes

$$\frac{d\langle \hat{n}_{k} \rangle}{dt} = -\sum_{k'} \Gamma_{k,k'} \langle \hat{n}_{k} \rangle \langle \hat{n}_{k'} \rangle$$

$$\Gamma_{k,k'} = \sum_{j} \frac{16g_{j}^{2}}{V} \frac{\gamma_{j}}{\gamma_{j}^{2} + (E_{j}/\hbar)^{2}} |k - k'|^{2}.$$
(A9)

Note that Eq. (A9) recovers the standard rate equations that describe direct chemical reactions, if we identify  $g_{\rm im} \equiv 3\pi \hbar b_{\rm im}^3/m = \sum_j 4g_j^2 \gamma_j/[\gamma_j^2 + (E_j/\hbar)^2]$  and  $g_{\rm re} \equiv 3\pi \hbar b_{\rm re}^3/m = \sum_j 4g_j^2 (E_j/\hbar)/[\gamma_j^2 + (E_j/\hbar)^2]$ , with  $b_{\rm re}^3$  and  $b_{\rm im}^3$  the real and imaginary parts of the scattering volume.

As mentioned in the main text, Eq. (A9) can be generalized to account for any type of trapping potentials V(r) by

replacing  $\langle \hat{n}_k \rangle$  by the population  $\langle \hat{n}_n \rangle$  as given by

$$\frac{d\langle \hat{n}_n \rangle}{dt} \approx -\sum_{n'} \Gamma_{nn'} \langle \hat{n}_n \rangle \langle \hat{n}_{n'} \rangle, \tag{A10}$$

where  $\Gamma_{nn'} \equiv 4\Gamma_{nn'nn'}$  with

$$\Gamma_{nn'n''n'''} = \frac{3\pi\hbar b_{\text{im}}^{3}}{m} \left( \int d\mathbf{r}^{3} \{ [\nabla \phi_{n}^{*}(\mathbf{r})] \phi_{n'}^{*}(\mathbf{r}) - \phi_{n}^{*}(\mathbf{r}) [\nabla \phi_{n''}^{*}(\mathbf{r})] \} \cdot \{ [\nabla \phi_{n''}(\mathbf{r})] \phi_{n''}(\mathbf{r}) - \phi_{n''}(\mathbf{r}) [\nabla \phi_{n'''}(\mathbf{r})] \} \right), \tag{A11}$$

where  $\phi_n(\mathbf{r})$  is the eigenfunction of the eigenmode  $\mathbf{n}$  of the single-particle Hamiltonian.

#### APPENDIX B: MEAN-FIELD APPROXIMATION

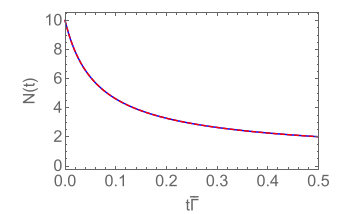
One approximation we make when we derive the rate equation in the paper [see Eq. (9) in the main text], is the mean-field approximation which assumes that

$$\frac{\langle \hat{n}_n \rangle}{dt} = -\sum_{m \neq n} \Gamma_{nm} \langle \hat{n}_n \hat{n}_m \rangle \approx -\sum_{m \neq n} \Gamma_{nm} \langle \hat{n}_n \rangle \langle \hat{n}_m \rangle, \quad (B1)$$

where the correlation  $\langle \hat{n}_n \hat{n}_m \rangle_c = \langle \hat{n}_n \hat{n}_m \rangle - \langle \hat{n}_n \rangle \langle \hat{n}_m \rangle$  between two particles is neglected. For an ideal Fermi gas, the magnitude of the initial correlations  $\sum_{m \neq n} \langle \hat{n}_n \hat{n}_m \rangle_c$  ranges between 0 (at T=0) and N (at  $T\to\infty$ ). Therefore the maximum correlation for each two-particle pair is roughly 1/N and is negligible for realistic systems consisting of  $\sim 10^4$  particles. In order to prove the validity of this mean-field approximation, we numerically compare the particle loss dynamics for ten particles with and without the correlation terms and we find no discernible difference between these two simulations as shown in Fig. 4.

To take into account the correlation terms, we use the cumulant expansion method which keeps track of two point correlations and truncate higher-order correlation terms. Specifically, three-point correlations are approximated as

$$\langle \hat{n}_{n} \hat{n}_{m} \hat{n}_{q} \rangle \approx \langle \hat{n}_{n} \hat{n}_{m} \rangle \langle \hat{n}_{q} \rangle + \langle \hat{n}_{n} \hat{n}_{q} \rangle \langle \hat{n}_{m} \rangle + \langle \hat{n}_{m} \hat{n}_{q} \rangle \langle \hat{n}_{n} \rangle - 2 \langle \hat{n}_{n} \rangle \langle \hat{n}_{m} \rangle \langle \hat{n}_{q} \rangle.$$
 (B2)



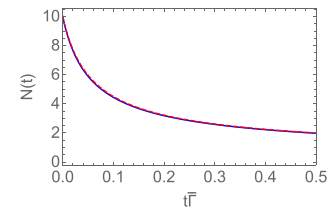


FIG. 4. Particle loss dynamics for ten particles in onedimensional homogeneous gas solved using the cumulant expansion (blue curve) and the mean-field approximation (red dashed curve) for  $T/T_F = 0.5$  (left) and  $T/T_F = 2$  (right).

Therefore, the set of exact equations, given by

$$\frac{\langle \hat{n}_{n} \rangle}{dt} = -\sum_{m \neq n} \Gamma_{nm} \langle \hat{n}_{n} \hat{n}_{m} \rangle,$$

$$\frac{\langle \hat{n}_{n} \hat{n}_{p} \rangle}{dt} = -\Gamma_{nm} \langle \hat{n}_{n} \rangle \langle \hat{n}_{m} \rangle - \sum_{m \neq n \neq p} (\Gamma_{np} + \Gamma_{mp}) \langle \hat{n}_{n} \hat{n}_{m} \hat{n}_{p} \rangle$$
(B3)

can be approximated as

$$\frac{\langle n_n \rangle}{dt} = -\sum_{m \neq n} \Gamma_{nm} (\langle \hat{n}_n \rangle \langle \hat{n}_m \rangle + \langle \hat{n}_n \hat{n}_m \rangle_c),$$

$$\frac{d \langle \hat{n}_n \hat{n}_m \rangle_c}{dt} = -\Gamma_{nm} (1 - \langle \hat{n}_n \rangle - \langle \hat{n}_m \rangle) (\langle \hat{n}_n \rangle \langle \hat{n}_m \rangle + \langle \hat{n}_n \hat{n}_m \rangle_c)$$

$$-\sum_{n \neq m \neq p} \Gamma_{np} (\langle \hat{n}_n \hat{n}_m \rangle_c \langle \hat{n}_p \rangle + \langle \hat{n}_m \hat{n}_p \rangle_c \langle \hat{n}_n \rangle)$$

$$-\sum_{n \neq m \neq p} \Gamma_{np} (\langle \hat{n}_n \hat{n}_m \rangle_c \langle \hat{n}_p \rangle + \langle \hat{n}_n \hat{n}_p \rangle_c \langle \hat{n}_m \rangle). (B4)$$

# APPENDIX C: GENERAL RATE EQUATIONS INCORPORATING THE INTERNAL DEGREES OF FREEDOM

So far we have ignored the internal degrees of freedom of complexes and molecules. Here we show that as long as the complex decay rate is the largest energy scale in the problem, we can ignore them. To show that, let us label all the other internal degrees of freedom (electronic state, vibration/rotation state, the spin state) of molecules and complexes with the vector *s*. After including them, the master equation to model the collision processes can be generalized from Eqs. (1)–(4) in the main text to the following equations:

$$\begin{split} \frac{d\hat{\rho}}{dt} &= \frac{i}{\hbar} [\hat{H}, \, \hat{\rho}] + \mathcal{L}(\hat{\rho}), \quad \hat{H} = \hat{H}_{\text{single}} + \hat{H}_{\text{int}}, \\ \hat{H}_{\text{single}} &= \sum_{j,k,s} E^b_{j,k,s} \hat{b}^\dagger_{j,k,s} \hat{b}_{j,k,s} + \sum_{k,s} E^c_{k,s} \hat{c}^\dagger_{k,s} \hat{c}_{k,s}, \\ \hat{H}_{\text{int}} &= \sum_{j,k,s,s',s''} \frac{\hbar g_{j,s,s'}}{\sqrt{V}} |\mathbf{k} - \mathbf{k}'| (\hat{b}^\dagger_{j,k+k',s''} \hat{c}_{k,s} \hat{c}_{k',s'} + \text{H.c.}), \\ \mathcal{L}(\hat{\rho}) &= \sum_{j,k,s} \gamma_j \mathcal{L}[\hat{b}_{j,k,s}] \, \hat{\rho}, \end{split}$$

where the single-particle energy  $E_{k,s}^{c(b)}$  also includes the internal energy.

Accordingly, the equations of motion for the relevant observables become

$$\frac{d\langle \hat{n}_{k,s}\rangle}{dt} = \sum_{j,k',s',s''} \frac{4g_{j,s,s',s''}}{\sqrt{V}} \times |\mathbf{k} - \mathbf{k}'| \operatorname{Im}[\langle \hat{b}_{j,k+k',s''}^{\dagger} \hat{c}_{k,s} \hat{c}_{k',s'}\rangle], \quad (C2)$$

$$\frac{d\langle \hat{b}_{j,k+k',s''}^{\dagger} \hat{c}_{k,s} \hat{c}_{k',s'}\rangle}{dt}$$

$$= -\gamma_{j}\langle \hat{b}_{j,k+k',s''}^{\dagger} \hat{c}_{k,s} \hat{c}_{k',s'}\rangle + i \frac{2g_{j,s,s',s''}}{+} i \frac{2g_{j,s,s',s''}}{\sqrt{V}}$$

$$\times |\mathbf{k} - \mathbf{k}'| \left( \langle \hat{n}_{j,k+k',s''}^{\dagger} \rangle - 2\langle \hat{n}_{k,s} \hat{n}_{k',s'} \rangle \right), \quad (C3)$$

$$\frac{d\langle \hat{n}_{j,k+k',s''}^{\dagger} \rangle}{dt} = -2\gamma_{j}\langle \hat{n}_{j,k+k',s''}^{\dagger} \rangle$$

$$-\frac{2}{\sqrt{V}} \sum_{k'} g_{j,s,s',s''} |\mathbf{k}' - \mathbf{k}|$$

$$\times \operatorname{Im}[\langle \hat{b}_{j,k+k',s''}^{\dagger} \hat{c}_{k,s} \hat{c}_{k',s'} \rangle]. \quad (C4)$$

Assuming the complex decay rate has the largest energy scale, the complex can be adiabatically eliminated and its steady-state population neglected. Therefore the complex-molecule correlation term can be approximated as

$$\langle \hat{b}_{j,k+k',s''}^{\dagger} \hat{c}_{k,s} \hat{c}_{k',s'} \rangle$$

$$\approx -i \frac{4g_{j,s,s',s''}}{\sqrt{V}} |k - k'| \langle \hat{n}_{k,s} \rangle \langle \hat{n}_{k',s'} \rangle / (\gamma - iE_{j,s,s',s''}/\hbar), \text{ (C5)}$$

where  $E_{j,s,s',s''} = E^c_{k+k',s''} - E^b_{k,s} - E^b_{k',s'}$ . There we have also ignored single-particle kinetic energy terms, hence  $E_{j,s,s',s''}$  is independent of k,k'. By substituting the correlations into the equation of motion for molecules, the generalized dynamics for the molecular population becomes

$$\frac{d\langle \hat{n}_{k,s}\rangle}{dt} \equiv -\sum_{k',s'} \Gamma_{k,k'}^{s,s'} \langle \hat{n}_{k,s}\rangle \langle \hat{n}_{k',s'}\rangle,$$

$$\Gamma_{k,k'}^{s,s'} = \sum_{j,s''} \frac{16g_{j,s,s',s''}^2}{V} \frac{\gamma_j}{\gamma_j^2 + (E_{j,s,s',s''}/\hbar)^2} |\mathbf{k} - \mathbf{k}'|^2,$$
(C6)

which takes a similar form as Eq. (A9).

#### APPENDIX D: EFFECTS OF ELASTIC SCATTERING

As discussed in the last section, both elastic and inelastic interactions are present. According to the multichannel quantum defect theory (MQDT) [11], the elastic and inelastic scattering volumes in KRb have exactly the same amplitude but with opposite sign. However, thermalization effect of the elastic collision cannot be captured by a second-order cumulant expansion such as the one used to derive Eq. (A4). Instead, here we use kinetic theory to incorporate thermalization processes induced by elastic collisions [23] and demonstrate that for the case of KRb they play a minimal role in the loss dynamics. In the context of kinetic theory the

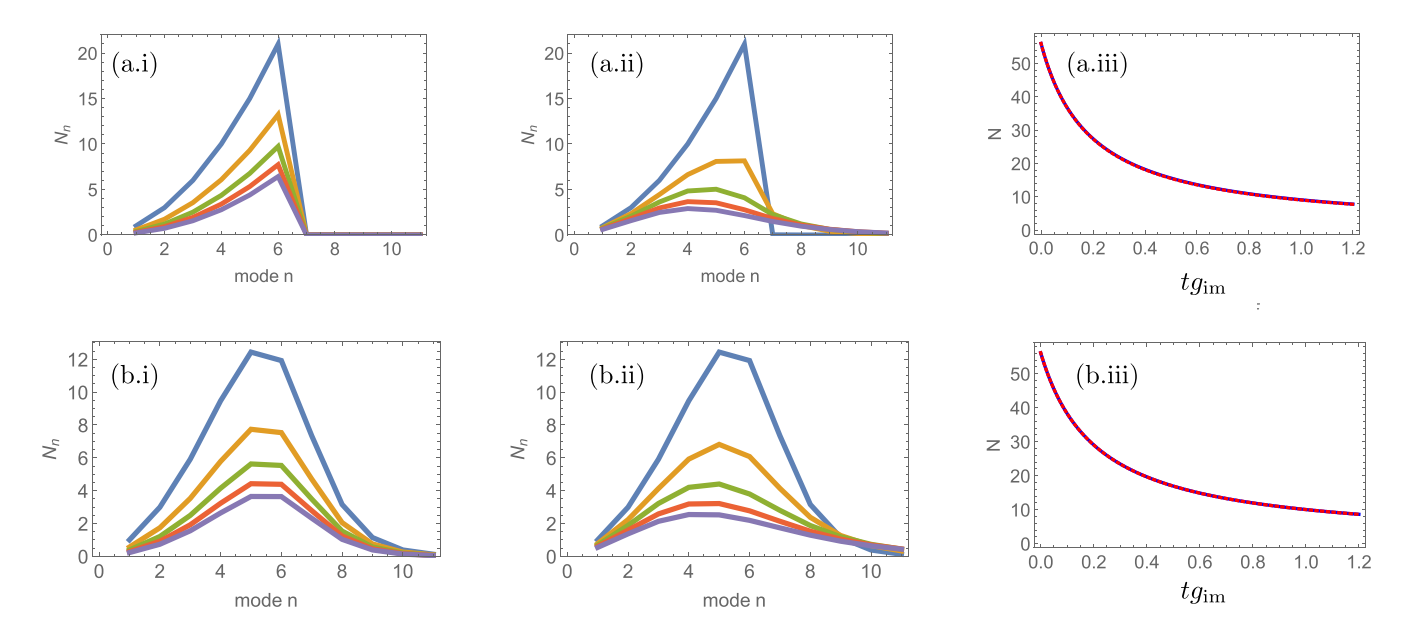


FIG. 5. Population dynamics for different elastic scattering volumes and temperatures: (a) T=0, (b)  $T=0.3T_F$ . Panels (i) and (ii) show the particle mode distribution for N(t=0)=56 particles  $(n=n_x+n_y+n_z)$  for  $g_{\rm re}=0$  and  $g_{\rm re}=-g_{\rm im}$ , respectively. The different colors represent the distribution at different times t. Blue: t=0; yellow:  $t=0.12g_{\rm im}$ ; green:  $t=0.24g_{\rm im}$ ; red:  $t=0.32g_{\rm im}$ ; and purple:  $t=0.48g_{\rm im}$ . Panel (iii) plots the dynamics of the particle number N(t) as a function of time (red:  $g_{\rm re}=0$ ; blue dashed:  $g_{\rm re}=-g_{\rm im}$ ). The comparison shows that the elastic collisions only slightly affect the decay rate by redistributing the density profile and do not affect the decay dynamics. To account for the fact that our simulations cannot be done for large systems, we capture the effect of the elastic interactions expected for the real particle number used in the experiment  $N_{\rm expt.}=10^4$ , by rescaling both  $g_{\rm re}$  and  $g_{\rm im}$  by a factor of  $(N_{\rm expt.}/56)^{-1/6}\approx 0.42$ , given the known scaling of  $\Gamma \propto N^{-1/6}$ .

rate equations read as

$$\frac{d\langle \hat{n}_{n} \rangle}{dt} = -\sum_{n'} \Gamma_{nn'} \langle \hat{n}_{n} \rangle \langle \hat{n}_{n'} \rangle 
+ \sum_{n'n''n'''} W_{nn'n''n'''} (\langle \hat{n}_{n''} \rangle \langle \hat{n}_{n'''} \rangle (1 - \langle \hat{n}_{n} \rangle) (1 - \langle \hat{n}_{n'} \rangle) 
- \langle \hat{n}_{n} \rangle \langle \hat{n}_{n'} \rangle (1 - \langle \hat{n}_{n''} \rangle) (1 - \langle \hat{n}_{n'''} \rangle),$$
(D1)

where  $W_{nn'n''n'''} = 2\pi/\omega |g_{\rm re}/g_{\rm im}|^2 |\Gamma_{nn'n''n'''}|^2 \delta_{E_n+E_{n'},E_{n''}+E_{n'''}}$  and  $E_n$  is the single-particle energy of mode n. Note that even though the elastic collisions are responsible for thermalization, the loss dynamics is mainly determined by the inelastic part since the elastic collisions conserve the total particle number and only slightly affect the decay rate by redistributing the mode population, as shown in Fig. 5.

# APPENDIX E: EVAPORATIVE HEATING

During the decay process, the evolution of the total energy of the system is given by

$$\frac{dE(t)}{dt} = -\sum_{\boldsymbol{n}_i, \boldsymbol{n}_i} E_{\boldsymbol{n}_i} \Gamma_{\boldsymbol{n}_i \boldsymbol{n}_j} \langle \hat{\boldsymbol{n}}_i \rangle_t \, \langle \hat{\boldsymbol{n}}_j \rangle_t \equiv -\overline{\Gamma \epsilon}(t) N(t)^2, \quad (E1)$$

where the time-dependent averaged particle decay rate is defined as  $\overline{\Gamma\epsilon}(t) = \sum_{n_i,n_i} \Gamma_{n_i n_j} E_{n_i} \langle \hat{n}_i \rangle_t \langle \hat{n}_j \rangle_t / N(t)^2$ . This equation together with the dynamics of N(t), can be used to solve for the dynamics of the energy density which

evolves as

$$d\epsilon(t)/dt = N[\overline{\Gamma}(t)\epsilon(t) - \overline{\Gamma}\epsilon(t)] \equiv \alpha_0 N \overline{\Gamma}\epsilon,$$
 (E2)

where  $\alpha_0 \equiv (\overline{\Gamma}\epsilon - \overline{\Gamma}\epsilon)/\overline{\Gamma}\epsilon$  denotes the evaporative cooling (heating) rate with negative (positive) value. For the 3D harmonic confinement under consideration, the particles with lower energy decay faster according to the scaling  $\Gamma \propto \epsilon^{-1/2}$ . Therefore the energy density increases as particles get lost and the system is evaporatively heated up. Using the numerical results in Fig. 6,  $\alpha_0$  is found to be a constant  $\alpha_0 = 0.07$  for all regimes down to  $T = 0.2T_F$  which is close to the result

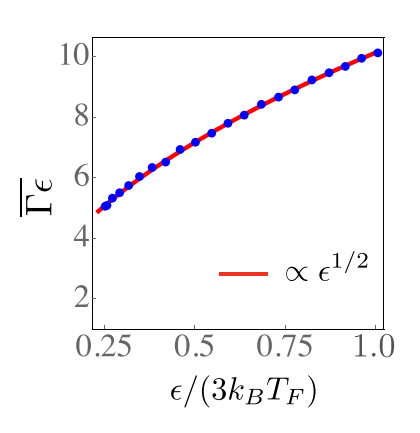


FIG. 6. The scaling relation  $\overline{\Gamma\epsilon} \propto \epsilon^{1/2}$  is valid over a wide range of  $\epsilon$  that covers both the classical limit and the quantum degenerate regime.

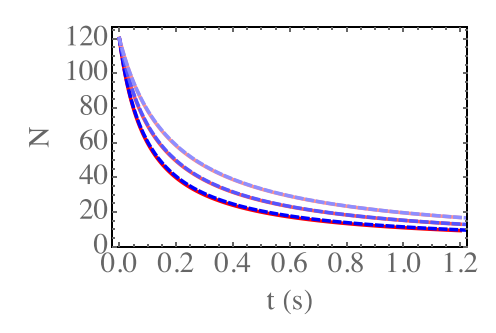


FIG. 7. Comparisons between the analytical results (red curves) and the numerical results (blue dashed lines) for the population dynamics at different initial equilibrium temperatures T=0,  $T=0.5T_F$ , and  $T=1.0T_F$  from bottom to top for N=120 particles. We find that the analytical results can well capture the numerically obtained dynamics over a wide range of temperatures.

 $\alpha_0 = 1/12$  in the classical regime predicted in [24] using a kinetic theory formalism.

## APPENDIX F: SIMPLIFIED ANALYTICAL EQUATIONS

The experiment measured the decay dynamics of an ensemble of  $N \sim 10^5$  particles, for which a quantitative theoretical comparison is numerically hard, even at the mean-field level. To overcome this numerical complexity as well as getting more insight into the decay, we assume that the decay dynamics is governed by simple analytical equations which are valid when the system is in equilibrium. Surprisingly, by performing comparisons with numerical calculations we find that these relations describe well the decay dynamics as shown in Fig. 7.

# APPENDIX G: INCORPORATING COMPLEX-MOLECULE COLLISIONS IN THE RATE EQUATIONS

Taking into account the complex-molecule collisions, the equations of motion for the relevant observables become

$$\frac{d\langle\hat{n}_{k}\rangle}{dt} = -\left(\sum_{j,k'} 2\alpha_{\gamma}\gamma_{j}/V\langle\hat{n}_{j,k'}^{b}\rangle\right)\langle\hat{n}_{k}\rangle + \sum_{j,k'} \frac{4g_{j}}{\sqrt{V}}|\mathbf{k} - \mathbf{k}'|\operatorname{Im}[\langle\hat{b}_{j,k+k'}^{\dagger}\hat{A}_{k,k'}\rangle] + \alpha_{g}\sum_{k''}\operatorname{Im}[\langle\hat{b}_{j,k+k'}^{\dagger}\hat{A}_{k,k'}\hat{n}_{k''}\rangle]/V, \qquad (G1)$$

$$\frac{d\langle\hat{b}_{j,k+k'}^{\dagger}\hat{A}_{k,k'}\rangle}{dt} = -\left[\gamma_{j}\left(1 + \alpha_{\gamma}/V\sum_{k''}\langle\hat{n}_{k''}\rangle\right) + \sum_{j',k''} 2\alpha_{\gamma}\gamma_{j'}/V\langle\hat{n}_{j',k''}^{b}\rangle\right]\langle\hat{b}_{j,k+k'}^{\dagger}\hat{A}_{k,k'}\rangle + i\frac{2g_{j}}{\sqrt{V}}|\mathbf{k} - \mathbf{k}'|\left(\langle\hat{n}_{j,k+k'}^{b}\rangle - 2\langle\hat{n}_{k}\hat{n}_{k'}\rangle\right) + i\frac{2g_{j}\alpha_{g}}{V^{3/2}}|\mathbf{k} - \mathbf{k}'|\sum_{k''}\left(\langle\hat{n}_{j,k+k'}^{b}\hat{n}_{k''}\rangle - 2\langle\hat{n}_{k}\hat{n}_{k'',k''}\rangle\right), \qquad (G2)$$

$$\frac{d\langle\hat{n}_{j,k}^{b}\rangle}{dt} = -2\gamma_{j}\left(1 + \alpha_{\gamma}\sum_{k'}\langle\hat{n}_{k'}\rangle/V\right)\langle\hat{n}_{j,k}^{b}\rangle - \frac{2g_{j}}{\sqrt{V}}\sum_{k'}|2\mathbf{k}' - \mathbf{k}|\left(\operatorname{Im}[\langle\hat{b}_{j,k}^{\dagger}\hat{A}_{k',k-k'}\rangle] + \alpha_{g}\sum_{k''}\operatorname{Im}[\langle\hat{b}_{j,k}^{\dagger}\hat{A}_{k',k-k'}\hat{n}_{k''}\rangle]\right), \qquad (G3)$$

where  $\hat{n}_{i,k}^b = \hat{b}_{i,k}^{\dagger} \hat{b}_{j,k}$  is the complex population operator.

Here we have neglected the kinetic energy term and the binding energy term. In addition, since the complex decay rate is large, it is fair to assume that the complex population can be neglected when it is compared to the molecule population. Therefore, by adiabatically eliminating the complex, one can obtain

$$\langle \hat{b}_{j,k+k'}^{\dagger} \hat{A}_{k,k'} \rangle = -i \frac{4g_{j}}{\sqrt{V}} (1 + \alpha_{g}n) |\mathbf{k} - \mathbf{k'}| \langle \hat{n}_{k} \rangle \langle \hat{n}_{k'} \rangle / [\gamma_{j} (1 + \alpha_{\gamma}n)],$$

$$\langle \hat{n}_{j,k}^{b} \rangle = -\frac{g_{j}}{\sqrt{V}} (1 + \alpha_{g}n) \sum_{k'} |2\mathbf{k'} - \mathbf{k}| \operatorname{Im}[\langle \hat{b}_{j,k}^{\dagger} \hat{A}_{k',k-k'} \rangle] / [\gamma_{j} (1 + \alpha_{\gamma}n)]$$

$$= \frac{4g_{j}^{2} (1 + \alpha_{g}n)^{2}}{V \gamma_{j}^{2} (1 + \alpha_{\gamma}n)^{2}} \sum_{k'} |2\mathbf{k'} - \mathbf{k}|^{2} \langle \hat{n}_{k-k'} \rangle \langle \hat{n}_{k'} \rangle,$$
(G5)

where  $n = \sum_{k} \langle \hat{n}_{k} \rangle / V$  is the density of the molecules.

Similarly, by substituting the correlations into Eq. (G1), the dynamics for the molecular population becomes

$$\frac{d\langle \hat{n}_{k} \rangle}{dt} = -\sum_{j,k'} \frac{16g_{j}^{2}(1 + \alpha_{g}n)^{2}}{V\gamma_{j}(1 + \alpha_{\gamma}n)} |\mathbf{k} - \mathbf{k}'|^{2} \langle \hat{n}_{k} \rangle \langle \hat{n}_{k'} \rangle 
- \sum_{j,k',k''} \frac{8\alpha_{\gamma}g_{j}^{2}(1 + \alpha_{g}n)}{V^{2}\gamma_{j}^{2}(1 + \alpha_{\gamma}n)^{2}} |2\mathbf{k}'' - \mathbf{k}'| \langle \hat{n}_{k} \rangle \langle \hat{n}_{k''} \rangle \langle \hat{n}_{k'-k''} \rangle 
\approx - \sum_{k'} \Gamma_{k,k'} \frac{(1 + \alpha_{g}n)^{2}}{(1 + \alpha_{\gamma}n)} \langle \hat{n}_{k} \rangle \langle \hat{n}_{k'} \rangle - \frac{1}{2} \sum_{j,k',k''} \frac{\alpha_{\gamma}}{V} \Gamma_{k'',k'-k''} \langle \hat{n}_{k} \rangle \langle \hat{n}_{k''} \rangle \langle \hat{n}_{k'-k''} \rangle.$$
(G6)

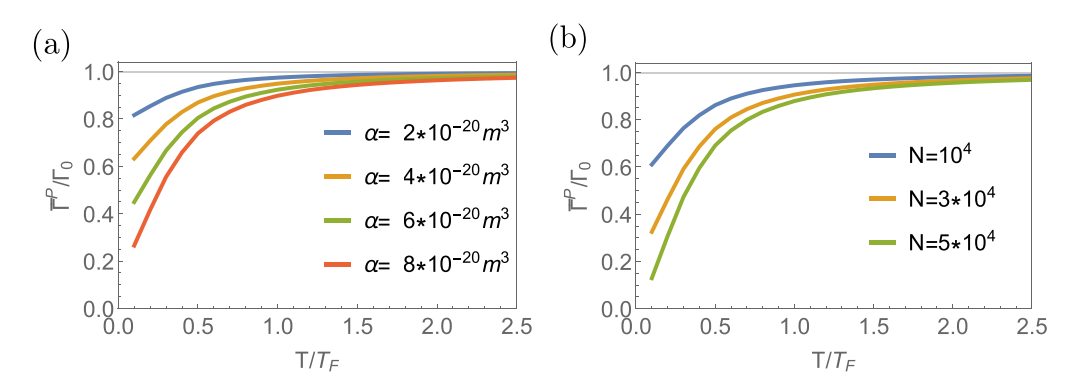


FIG. 8. The plots show  $\overline{\Gamma}_P/\Gamma_0$  for different (a)  $\alpha$  values assuming  $N=2\times 10^4$  and (b) different particle number N setting  $\alpha=6\times 10^{-20}$  m<sup>3</sup>.

Here we have assumed  $\alpha_{g(\gamma)}n \ll 1$  approximation that is found to be valid for the KRb experimental parameters. In addition, we assume  $\gamma_j \gg E_j$  since only the close to resonance complex can be formed.

And the dynamical equation for the total number of the molecules is given by

$$\frac{dN}{dt} = -\sum_{k,k'} \Gamma_{k,k'} (1 + 2\alpha_g n - \alpha_\gamma n/2) \langle \hat{n}_k \rangle \langle \hat{n}_{k'} \rangle. \quad (G7)$$

By comparing Eq. (G6) with Eq. (A9), we find the modified decay rate after taking into account the inelastic molecule-complex collisions becomes

$$\Gamma_{k,k'}^P = \Gamma_{k,k'}(1 + 2\alpha_g n - \alpha_\gamma n/2), \tag{G8}$$

indicating that the effective inelastic scattering parameter becomes

$$g_{\rm im}^P = g_{\rm im}(1 + 2\alpha_g n - \alpha_\gamma n/2). \tag{G9}$$

## APPENDIX H: REVISED DECAY RATES

In a harmonic trap, the density of the gas is not homogeneous, therefore the spatial dependence of the effective scattering coefficient  $g_{\text{im}}^P(\mathbf{r})$  needs to be taken into account. This leads to a revised decay rate  $\Gamma_{n_i n_j n_k n_l}$  given by

$$\Gamma_{nn'n''n'''}^{P} = \int d\mathbf{r}^{3} g_{\text{im}}^{P}(\mathbf{r}) \{ [\nabla \phi_{n}^{*}(\mathbf{r})] \phi_{n'}^{*}(\mathbf{r}) - \phi_{n}^{*}(\mathbf{r}) [\nabla \phi_{n'}^{*}(\mathbf{r})] \} \cdot \{ [\nabla \phi_{n''}(\mathbf{r})] \phi_{n'''}(\mathbf{r}) - \phi_{n''}(\mathbf{r}) [\nabla \phi_{n'''}(\mathbf{r})] \}.$$
(H1)

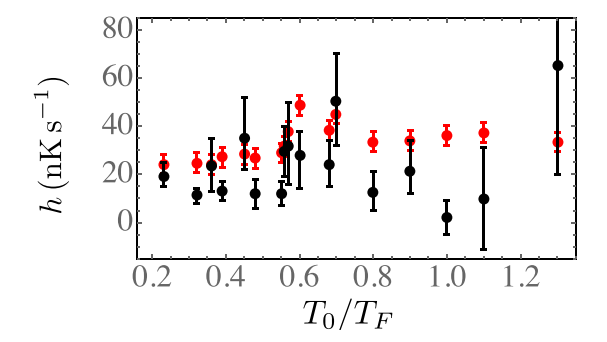


FIG. 9. Comparison between the theoretically predicted (red dots) and the experimentally measured (black dots) heating rates.

Consequently, the revised rate equations for the mode populations are given by

$$\frac{d\langle \hat{n}_{n}\rangle}{dt} \approx -\sum_{n'} \Gamma_{nn'} \langle \hat{n}_{n}\rangle \langle \hat{n}_{n'}\rangle, \tag{H2}$$

where  $\Gamma^{P}_{nn'} \equiv 4\Gamma^{P}_{nn'nn'}$ .

The scaling of  $\overline{\Gamma}^P$  for systems with a large number of particles is limited by the computation complexity. To overcome this limit, here we instead take the local density approximation starting from a semiclassical phase space distribution given by

$$f(\mathbf{r}, \mathbf{p}) = \frac{1}{\exp\left[\left(\frac{m\omega^2 \mathbf{r}^2}{2} + \frac{\mathbf{p}^2}{2m} - \mu\right)/k_B T\right] + 1},$$
 (H3)

the averaged decay rate can be calculated as

$$\overline{\Gamma}^P = \frac{\int g_{\text{im}}^P(\mathbf{r}) \mathbf{p}^2 f(\mathbf{r}, \mathbf{p}) d\mathbf{r}^3 d\mathbf{p}^3}{NV},$$
(H4)

where N and V denote the particle number and the volume, respectively, and the first term in the integrand  $g_{\text{im}}^{P}(\mathbf{r})$  accommodates the spatial dependence, the second term  $\mathbf{p}^{2}$  represents the p-wave collisional kernel that is proportional to the kinetic energy of the gas, and the denominator is simply the total particle number of the system.

We compute the integral Eq. (H4) numerically assuming different  $\alpha$  and particle number N. As shown in Fig. 8, we find that the ratio  $\overline{\Gamma}_P/\Gamma_0$ , assuming  $\alpha=0$ , saturates at high temperature and gets suppressed as the gas enters quantum degeneracy [ $\Gamma_0$  is calculated using Eq. (H4)]. In addition, the degree of suppression and the saturation temperature increase with increasing particle number.

#### APPENDIX I: FITTING ANALYSIS

In the experiment, the molecules are created and cooled down to the Fermi degenerate regime. By fitting the initial density profile to a Fermi-Dirac distribution, the initial temperatures  $T_0^{\rm ex}$  and  $T_0^{\rm ex}/T_F$  are obtained. To keep track of the reactive collision processes, the particle number  $N^{\rm ex}(t)$  and the volume  $V^{\rm ex}(t)$  are measured as a function of the evolution time t. To compare with the experimentally extracted decay rate, both the experimental initial energy density and the initial particle number are needed as input parameters for the theory. They are extracted by a fitting procedure: By fitting  $V^{\rm ex}(t)$  to  $V(t) = [4\pi \epsilon(t)/3m\overline{\omega}^2]^{3/2}$ , the initial energy density

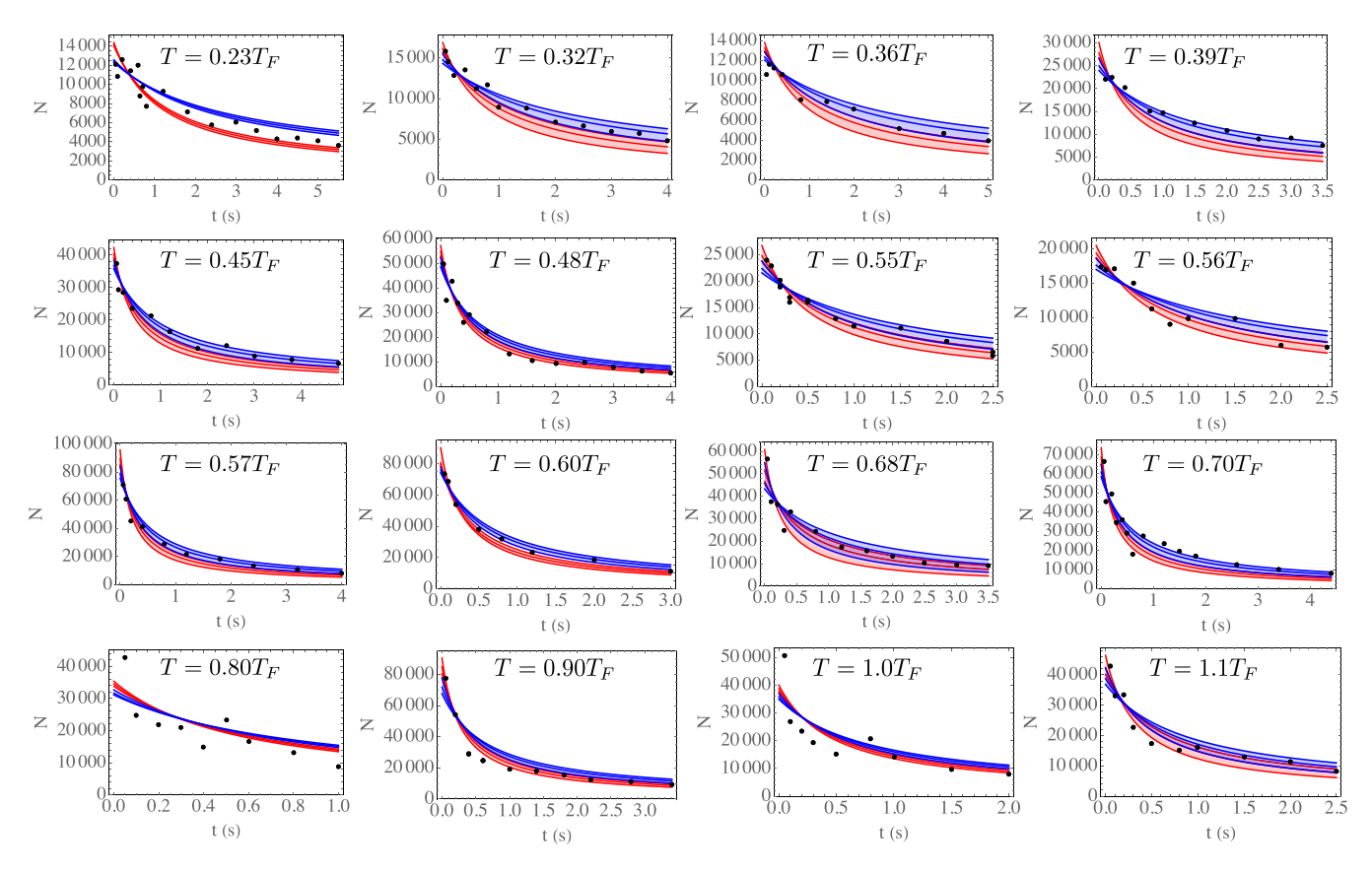


FIG. 10. Comparison between theoretical results and experimental data (black dots) for the particle number N(t). The theoretical results are obtained using the decay rates [red (light-gray/lower) bands]  $\overline{\Gamma}_0^{\text{th}}$  and the revised decay rates [blue (dark-gray/upper) bands]  $\overline{\Gamma}_0^{\text{th},P} = \overline{\Gamma}_0^{\text{th}}(\overline{\Gamma}^P/\Gamma_0)$ , respectively, where the ratio  $\overline{\Gamma}^P/\Gamma_0$  is calculated assuming  $\alpha = 8 \times 10^{-20} \, \text{m}^3$ .

 $\epsilon_0^{\rm ex} \pm \Delta \epsilon^{\rm ex}$  and the linear heating rate  $h^{\rm ex} \pm \Delta h^{\rm ex}$  can be extracted with  $\Delta \epsilon^{\rm ex}$  and  $\Delta h^{\rm ex}$  the uncertainties. Furthermore, by finding the best fit of  $N^{\rm ex}(t)$  to the theoretical  $N^{\rm th}(t)$  obtained, the initial particle number  $N_0^{\rm ex} \pm \Delta N_0^{\rm ex}$  can be obtained.

the initial particle number  $N_0^{\rm ex} \pm \Delta N_0^{\rm ex}$  can be obtained. Assuming  $\alpha_0 = 0.07$  and  $h_{\rm bg} = 20 \pm 4$  nK/s, together with the extracted parameters  $N_0^{\rm ex}$ ,  $\epsilon_0^{\rm ex}$  can be solved self-consistently. The theoretically predicted  $h^{\rm th}$  is extracted from a linear fit to  $\epsilon^{\rm th}(t)$ . The comparison of the theoretically predicted  $h^{\rm th}$  and the experimentally measured  $h^{\rm ex}$  are shown in Fig. 9. We find that for the fixed  $h_{\rm bg}$  used in the theory model, the theory results roughly agree with the experimental ones in the degenerate regime where the density is high, while the theory overestimates the heating rates in the classical regime where the density is low, which is qualitatively consistent with the conjecture that the background heating is induced by the

density-dependent collisions and should be smaller for dilute systems.

The theory predicted N(t) is obtained by substituting theoretically calculated decay rate  $\overline{\Gamma}_0^{\text{th}}$ , the heating rate  $h^{\text{th}}$ , and the experimentally measured initial conditions  $\epsilon_0^{\text{ex}}$  and  $N_0^{\text{ex}}$  into Eq. (12) in the main text. In Fig. 10, we compare the dynamics of N(t) predicted by the theoretical results and the experimental data. The decay rate  $\beta_0$  is obtained as the best fit of the theoretical n(t) = N(t)/V(t) to Eq. (12) in the main text.

To incorporate the effect of the formation of the complex, we replace  $\overline{\Gamma}_0^{th}$  by  $\overline{\Gamma}_0^{th,P}=\overline{\Gamma}_0^{th}(\overline{\Gamma}^P/\overline{\Gamma}_0)$ . Since  $\overline{\Gamma}^P/\overline{\Gamma}_0$  gives rise to suppression, the agreement between the dynamics of the particle number of the theoretical results and experimental data becomes better, as shown in Fig. 10.

<sup>[1]</sup> L. De Marco, G. Valtolina, K. Matsuda, W. G. Tobias, J. P. Covey, and J. Ye, A degenerate Fermi gas of polar molecules, Science **363**, 853 (2019).

<sup>[2]</sup> L. D. Carr, D. DeMille, R. V. Krems, and J. Ye, Cold and ultracold molecules: Science, technology and applications, New J. Phys. 11, 055049 (2009).

<sup>[3]</sup> S. A. Moses, J. P. Covey, M. T. Miecnikowski, D. S. Jin, and J. Ye, New frontiers for quantum gases of polar molecules, Nat. Phys. 13, 13 (2017).

<sup>[4]</sup> S. A. Moses, J. P. Covey, M. T. Miecnikowski, B. Yan, B. Gadway, J. Ye, and D. S. Jin, Creation of a low-entropy quantum gas of polar molecules in an optical lattice, Science 350, 659 (2015).

<sup>[5]</sup> L. Anderegg, B. L. Augenbraun, Y. Bao, S. Burchesky, L. W. Cheuk, W. Ketterle, and J. M. Doyle, Laser cooling of optically trapped molecules, Nat. Phys. 14, 890 (2018).

<sup>[6]</sup> S. Ospelkaus, K.-K. Ni, D. Wang, M. H. G. de Miranda, B. Neyenhuis, G. Quéméner, P. S. Julienne, J. L. Bohn, D. S.

- Jin, and J. Ye, Quantum-state controlled chemical reactions of ultracold potassium-rubidium molecules, Science **327**, 853 (2010).
- [7] H. A. Bethe, Theory of disintegration of nuclei by neutrons, Phys. Rev. 47, 747 (1935).
- [8] E. P. Wigner, On the behavior of cross sections near thresholds, Phys. Rev. **73**, 1002 (1948).
- [9] H. R. Sadeghpour, J. L. Bohn, M. J. Cavagnero, B. D. Esry, I. I. Fabrikant, J. H. Macek, and A. R. P. Rau, Collisions near threshold in atomic and molecular physics, J. Phys. B: At., Mol. Opt. Phys. 33, R93 (2000).
- [10] C. H. Greene, A. R. P. Rau, and U. Fano, General form of the quantum-defect theory. II, Phys. Rev. A 26, 2441 (1982).
- [11] Z. Idziaszek and P. S. Julienne, Universal Rate Constants for Reactive Collisions of Ultracold Molecules, Phys. Rev. Lett. 104, 113202 (2010).
- [12] M.-G. Hu, Y. Liu, D. D. Grimes, Y.-W. Lin, A. H. Gheorghe, R. Vexiau, N. Bouloufa-Maafa, O. Dulieu, T. Rosenband, and K.-K. Ni, Direct observation of bimolecular reactions of ultracold KRb molecules, Science 366, 1111 (2019).
- [13] Y. Liu, M.-G. Hu, M. A. Nichols, D. D. Grimes, T. Karman, H. Guo, and K.-K. Ni, Photo-excitation of long-lived transient intermediates in ultracold reactions, Nat. Phys. 16, 1132 (2020).
- [14] J. F. E. Croft, J. L. Bohn, and G. Quéméner, Unified model of ultracold molecular collisions, Phys. Rev. A 102, 033306 (2020).
- [15] P. S. Julienne, Ultracold molecules from ultracold atoms: A case study with the KRb molecule, Faraday Discuss. 142, 361 (2009).

- [16] B. Misra and E. C. G. Sudarshan, The Zeno's paradox in quantum theory, J. Math. Phys. 18, 756 (1977).
- [17] W. M. Itano, D. J. Heinzen, J. J. Bollinger, and D. J. Wineland, Quantum Zeno effect, Phys. Rev. A 41, 2295 (1990).
- [18] B. Zhu, B. Gadway, M. Foss-Feig, J. Schachenmayer, M. L. Wall, K. R. A. Hazzard, B. Yan, S. A. Moses, J. P. Covey, D. S. Jin, J. Ye, M. Holland, and A. M. Rey, Suppressing the Loss of Ultracold Molecules Via the Continuous Quantum Zeno Effect, Phys. Rev. Lett. 112, 070404 (2014).
- [19] A. Urvoy, Z. Vendeiro, J. Ramette, A. Adiyatullin, and Vladan Vuletić, Direct Laser Cooling to Bose-Einstein Condensation in a Dipole Trap, Phys. Rev. Lett. 122, 203202 (2019).
- [20] P. D. Gregory, J. A. Blackmore, S. L. Bromley, and S. L. Cornish, Loss of Ultracold <sup>87</sup>Rb<sup>133</sup>Cs Molecules Via Optical Excitation of Long-Lived Two-Body Collision Complexes, Phys. Rev. Lett. **124**, 163402 (2020).
- [21] B. D. Esry, C. H. Greene, and J. P. Burke, Recombination of Three Atoms in the Ultracold Limit, Phys. Rev. Lett. **83**, 1751 (1999).
- [22] B. D. Esry, Chris H. Greene, and H. Suno, Threshold laws for three-body recombination, Phys. Rev. A 65, 010705(R) (2001).
- [23] M. Holland, J. Williams, and J. Cooper, Bose-Einstein condensation: Kinetic evolution obtained from simulated trajectories, Phys. Rev. A 55, 3670 (1997).
- [24] K.-K. Ni, S. Ospelkaus, D. Wang, G. Quéméner, B. Neyenhuis, M. H. G. de Miranda, J. L. Bohn, J. Ye, and D. S. Jin, Dipolar collisions of polar molecules in the quantum regime, Nature (London) 464, 1324 (2010).